FD-DCNN: A Fourier Domain Denoising Convolutional Neural Network for Cardiac Artifact Removal in Single Channel EEG Signals

R. Acharjee, A. Paul and S. R. Ahamed

Department of EEE, Indian Institute of Technology Guwahati, Assam, India
{a.raktim, aditipaul, rafiahamed}@iitg.ac.in

***Abstract*— Electroencephalogram (EEG) signals are often contaminated by cardiac artifacts, which can significantly degrade the performance of downstream analysis. This paper presents a Fourier Domain Denoising Convolutional Neural Network (FD-DCNN) that leverages frequency domain convolution to effectively suppress electrocardiogram (ECG) artifacts in single channel EEG signals. Unlike conventional, time domain CNN-based approaches, the proposed model operates entirely in the spectral domain, replacing computationally expensive convolutions with element-wise complex multiplications, suitable for area and power constrained biomedical hardware. A complex-domain non-linear activation, PhaseReLU, is introduced after each spectral convolution to preserve magnitude while enabling non-linear feature extraction. The network is trained using a Morphology Preserving Loss (MPL) combining mean squared error and correlation to maintain amplitude fidelity and waveform morphology. The publicly available EEGdenoiseNet and MIT-BIH Polysomnographic databases were used to generate the simulated dataset for model training and evaluation. FD-DCNN achieves a lower Relative Root Mean Square Error (RRMSE) of 0.4301 in the time domain and 0.3548 in the frequency domain, along with a higher correlation coefficient of 0.8879, while requiring only 0.67M parameters, 2.5MB of memory, and 2.31M floating point operations per second (FLOPs), which is substantially less than a comparable time domain CNN with similar architecture. These results establish FD-DCNN as a lightweight, high-performance denoising architecture well-suited for efficient hardware implementation and real-time EEG processing.**

Keywords*— *Electroencephalogram (EEG), Fourier, Cardiac Artifacts, ECG, Convolutional Neural Network (CNN).

I. Introduction

Electroencephalography (EEG) is a non-invasive neurophysiological recording technique that measures the electrical activity of the brain with high temporal resolution [1][2]. However, EEG signals are inherently low in amplitude and highly susceptible to contamination from various physiological and environmental artifacts and noises [3]. Cardiac artifacts are captured in EEG recordings due to the volume conduction of the electrical activity of the heart through body tissues, allowing the strong electrocardiogram (ECG) potential to propagate to scalp electrodes [4]. ECG artifacts manifest as large-amplitude, quasi-periodic waveforms that overlap with the EEG in both time and frequency domains. Their spectral energy extends into low and mid-frequency EEG bands, corrupting neural features essential for accurate analysis [5]. Thus, removing these artifacts is crucial for downstream neural signal processing pipelines. Single channel EEG enables portable and computationally efficient brain monitoring but lacks spatial diversity, making artifact removal more challenging than in multichannel EEG [6].

Several approaches have been proposed for ECG artifact removal from single channel EEG, particularly in the absence of a coherent ECG reference [7]. Early works relied on energy-based QRS detection followed by subtraction techniques, such as ensemble average subtraction (EAS) [4] or adaptive filtering [8], but these often suffered from over or under-correction and high computational cost. Jiang et al. [9] later developed a fully automated wavelet-based method without requiring an ECG reference, achieving better detection accuracy and high correlation. Patel et al. [10] subsequently proposed an EEMD-based regression approach that suppresses cardiac artifacts while minimizing spectral distortion. Dora and Biswal [5] proposed a modified S-transform (MST)-based method to improve QRS localization accuracy, combined with a modified EAS to reduce overcompensation. Their approach demonstrated superior detection and correction performance over CWT and EEMD methods. In subsequent work, they introduced a correlation-based framework using modified variational mode decomposition (mVMD) [11]. This method exploits correlation among band-limited IMFs to identify artifacts without requiring R-R interval estimation, achieving high correlation while reducing computational complexity compared to EEMD-based algorithms.

Recent advances in data-driven learning have led to the development of several neural architectures for artifact suppression. Behera et al. [12] employed a Random Vector Functional Link Network (RVFLN) with recursive least squares learning to adaptively remove ECG artifacts, achieving enhanced SNR and improved spectral fidelity. Kalita et al. [13] proposed AnEEG, an LSTM-based GAN that effectively suppresses multiple physiological artifacts and outperforms wavelet-based methods. Among deep architectures, CNNs remain the most widely adopted due to their ability to hierarchically capture localized temporal features [14]. Compared to recurrent or adversarial models, CNNs provide a more hardware-efficient structure with inherently parallelizable operations, making them suitable for real-time and embedded implementations. However, traditional time domain CNNs perform convolution through sliding

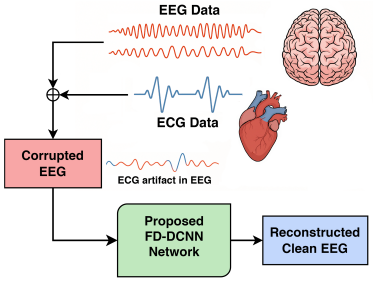

Figure 1. Flowchart of the proposed method.

kernels, resulting in high computational complexity ($O(N \cdot K)$ for signal length N and kernel size K) [15]. Furthermore, their limited receptive field often requires deeper or dilated layers for long-range dependencies, and the implicit learning of spectral filters is inefficient for frequency-specific artifacts. Pratt et al. [16] demonstrated that performing convolution entirely in the Fourier domain can significantly reduce computation while maintaining accuracy. Han et al. [15] further advanced this concept by introducing an efficient Fourier CNN with random kernels and a novel activation function, achieving faster training and reduced parameter count without sacrificing performance. These developments motivate exploration of frequency domain, low-complexity, and hardware-efficient implementations.

In this work, we propose a Fourier Domain Denoising Convolutional Neural Network (FD-DCNN), which exploits the Convolution Theorem to transform convolutions into element-wise multiplications in the spectral domain. This reduces complexity and provides explicit frequency domain representation for targeted artifact removal, and achieves parameter efficiency, critical for real-time, resource-constrained applications like portable EEG systems [17]. The architecture also integrates complex domain non-linear activation, residual learning, and a morphology-aware loss function to preserve EEG signal integrity while effectively suppressing the artifacts. The model is trained and evaluated using the simulated synthetic EEG dataset. Figure 1 illustrates the flowchart of the proposed method. The main contributions of this work are as follows:

1) A lightweight Fourier domain denoising CNN that operates entirely in the spectral domain, reducing computational cost, memory usage, and latency compared to time domain CNNs.
2) Complex domain feature extraction using PhaseReLU after each spectral convolution to preserve magnitude while enabling non-linear phase transformations for improved cardiac artifact suppression.
3) A morphology-preserving loss function that combines mean squared error and correlation to jointly preserve amplitude fidelity and waveform morphology.

The paper is structured as follows: Section II outlines the methods, covering the architecture of the proposed model, and performance evaluation metrics. Section III details data preprocessing, model training protocols, and an in-depth analysis of the results. Section IV concludes the paper with a discussion of the findings and their broader implications.

II. Methods

In this section, we first describe the architecture of the proposed FD-DCNN model, followed by a discussion of the metrics used for performance evaluation.

II-A. FD-DCNN Architecture

The proposed FD-DCNN network is designed to remove cardiac artifacts from single channel EEG signals by performing all convolutional operations directly in the frequency domain. The overall architecture is shown in Figure 2. FD-DCNN replaces conventional time domain convolutions with efficient element-wise complex multiplications in the spectral domain [18]. The process begins by transforming the input EEG signal $x(n)$ from the time domain to the frequency domain using the Discrete Fourier Transform (DFT) [19]:

$$X(k) = \sum_{n=0}^{N-1} x(n) e^{-j2\pi kn/N} \tag{1}$$

The DFT of a signal of length N has computational complexity $O(N^2)$, but the Fast Fourier Transform (FFT) algorithm [20] reduces this to $O(N \log N)$, providing a significant computational speed-up [21].

Let $X(\omega)$ and $H(\omega)$ denote the Fourier transform of the input signal and the learnable convolutional kernel, respectively. Instead of transforming time domain kernels into the frequency domain, FD-DCNN directly initializes and learns complex-valued kernels in the spectral domain using Glorot initialization [22]. This approach eliminates redundant kernel FFT computations and ensures that all learnable parameters are optimized for spectral operations.

According to the Convolution Theorem, convolution in the time domain corresponds to element-wise multiplication in the frequency domain [23]:

$$y(n) = (x(n) * h(n)) \xleftrightarrow{\mathcal{F}} Y(\omega) = X(\omega) \odot H(\omega) \tag{2}$$

where $\odot$ denotes complex Hadamard pointwise multiplication. Both $X(\omega)$ and $H(\omega)$ are complex-valued, therefore, the multiplication is carried out in the complex domain, with real and imaginary components learned and stored separately as $H_R(\omega)$ and $H_I(\omega)$. This complex multiplication effectively performs the convolution operation without explicit sliding-window computations and enables global frequency domain learning. Each kernel has a length of N, the same as

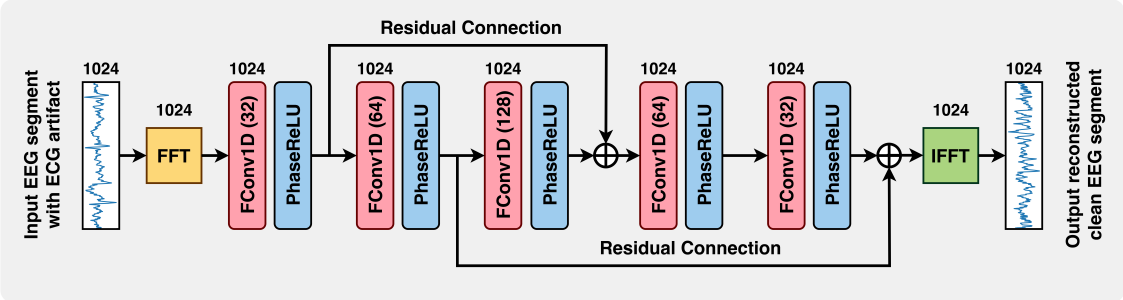

Figure 2. The architecture of the proposed Fourier Domain Denoising Convolutional Neural Network (FD-DCNN).

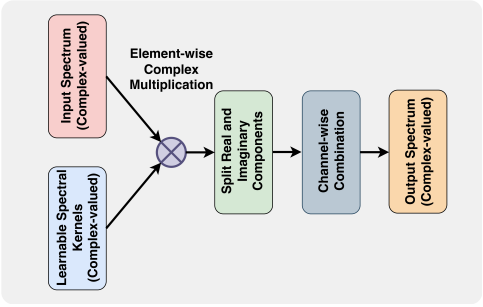

Figure 3. Block diagram of the FConv1D layer.

the FFT size, ensuring full-band spectral interaction and consistent dimensionality across layers.

The complete FD-DCNN architecture consists of a single FFT input transformation, five stacked Fourier Convolution (FConv1D) blocks, residual skip connections, an inverse FFT reconstruction stage, and a learnable output scaling layer. The FFT and IFFT are computed only once each for the entire network (before the first FConv1D and after the last FConv1D block), while all intermediate operations occur directly in the Fourier domain, significantly reducing computational overhead. In the first three FConv1D layers, the number of complex filters increases progressively ($32 \rightarrow 64 \rightarrow 128$) to capture diverse spectral structures and artifact patterns. The subsequent layers ($64 \rightarrow 32$) refine these features and suppress residual interference. In each FConv1D layer, multiple complex-valued filters are applied in parallel to the input spectrum, producing a set of complex feature maps. Let the input to a Fourier convolutional layer be $Z_{\text{in}}(\omega) \in \mathbb{C}^N$, and suppose the layer has F complex-valued filters:

$$W_k(\omega) = W_{k,R}(\omega) + jW_{k,I}(\omega) \tag{3}$$

where $k = 1, 2, \ldots, F$. After element-wise complex multiplication, the k-th filter output is:

$$U_k(\omega) = Z_{\text{in}}(\omega) \odot W_k(\omega) \tag{4}$$

This can be optimized using 3 multipliers and 2 adders as [24][25]. Each $U_k(\omega)$ is separated into its real and imaginary parts:

$$U_{k,R}(\omega) = \Re\{U_k(\omega)\}, \quad U_{k,I}(\omega) = \Im\{U_k(\omega)\} \tag{5}$$

These real and imaginary feature maps from all F filters are then stacked along the channel dimension and combined, producing a single complex-valued output spectrum per layer:

$$\begin{aligned} Y_R(\omega) &= \sum_{k=1}^{F} \alpha_{k,R} U_{k,R}(\omega) \\ Y_I(\omega) &= \sum_{k=1}^{F} \alpha_{k,I} U_{k,I}(\omega) \end{aligned} \tag{6}$$

where $\alpha_{k,R}$ and $\alpha_{k,I}$ are the learnable mixing weights for the real and imaginary channels, respectively. The final combined complex spectrum is:

$$Y(\omega) = Y_R(\omega) + jY_I(\omega) \tag{7}$$

This step aggregates all spectral responses and produces the complex-valued output of each layer. Block diagram of the FConv1D layer is shown in Figure 3.

Following the spectral convolution, a Phase Rectified Linear Unit (PhaseReLU) activation is applied. For a complex-valued spectral coefficient $z = |z|e^{j\phi_z}$, PhaseReLU preserves the magnitude $|z|$ and applies a rectification to the phase ϕ_z [15]:

$$\begin{aligned} PhaseReLU(z) = |z|(&\cos(ReLU(\phi_z)) \\ &+ i\sin(ReLU(\phi_z))) \end{aligned} \tag{8}$$

This non-linearity suppresses components with negative phase while retaining positive-phase information, thereby enabling non-linear feature extraction without distorting spectral magnitudes. Residual skip connections are introduced to preserve uncorrupted spectral components and improve gradient flow during training [26]. After the final Fourier convolutional block, the denoised complex spectrum is transformed back into the time domain using the inverse FFT:

$$\hat{x}(n) = \Re\{\text{IFFT}(Y(\omega))\} \tag{9}$$

As EEG is a real-valued signal, only the real component is retained. Finally, a learnable scaling factor η is applied to adjust the amplitude:

$$\hat{x}_{\text{scaled}}(n) = \eta \cdot \hat{x}(n) \tag{10}$$

The resulting $\hat{x}_{\text{scaled}}(n)$ represents the cleaned EEG segment with significantly reduced cardiac interference. Since FD-DCNN performs a single FFT and IFFT for the entire network and employs $L = 5$ layers of point-wise spectral multiplications, its total computational complexity is $O(2 \cdot N \log N + L \cdot N)$. In contrast, a conventional time domain CNN with equivalent architecture, depth, and kernel configuration has a complexity of $O(L{\cdot}N{\cdot}K)$. Thus, FD-DCNN achieves over an order-of-magnitude reduction in computation while preserving spectral fidelity.

II-B. Morphology Preserving Loss (MPL)

The FD-DCNN is trained using a custom Morphology Preserving Loss (MPL) function that combines the Mean Squared Error (MSE) with a correlation-based similarity term. The MSE component penalizes amplitude deviations between the predicted denoised EEG $\hat{x}(n)$ and the clean reference EEG $x_{\text{clean}}(n)$ [27]:

$$\mathcal{L}_{\text{MSE}} = \frac{1}{N}\sum_{n=1}^{N}\left(x_{\text{clean}}(n) - \hat{x}(n)\right)^2 \tag{11}$$

The correlation term measures the normalized inner product between the prediction and reference, encouraging the network to preserve signal morphology [28]:

$$\mathcal{L}_{\text{corr}} = \frac{\langle x_{\text{clean}}, \hat{x}\rangle}{\|x_{\text{clean}}\|\,\|\hat{x}\|} \tag{12}$$

The overall MPL loss is then expressed as:

$$\mathcal{L} = \mathcal{L}_{\text{MSE}} - \lambda\mathcal{L}_{\text{corr}} \tag{13}$$

where λ is a hyperparameter. This formulation ensures that the network not only minimizes reconstruction error but also maximizes structural similarity between the cleaned and reference EEG signals.

II-C. Performance Metrics

To assess the effectiveness of the proposed FD-DCNN in suppressing ECG artifacts in single channel EEG, the following quantitative performance metrics were employed:

II-C1. Relative Root Mean Square Error (RRMSE)

RRMSE quantifies the amplitude deviation between the denoised output $\tilde{z}$ and ground-truth reference EEG z, providing a measure of denoising accuracy [29]:

$$RRMSE_t = \frac{RMS(z - \tilde{z})}{RMS(\tilde{z})} \tag{14}$$

$$RRMSE_f = \frac{RMS(PSD(z) - PSD(\tilde{z}))}{RMS(PSD(\tilde{z}))} \tag{15}$$

where $RRMSE_t$ and $RRMSE_f$ are the temporal and spectral domain RRMSE, respectively, and PSD refers to the Power Spectral Density.

II-C2. Correlation Coefficient (CC)

The Pearson correlation coefficient assesses waveform and morphological similarity between z and $\tilde{z}$, reflecting how well the neural dynamics are preserved [29]:

$$CC = \frac{cov(z, \tilde{z})}{\sigma_{zz}\sigma_{\tilde{z}\tilde{z}}} \tag{16}$$

where $cov(\cdot)$ denotes the covariance between z and $\tilde{z}$, and $\sigma_{(\cdot)}$ represents their respective variances.

II-C3. Average Power Ratio (APR)

The APR quantifies the proportion of energy contained within a specific frequency band relative to the total energy across the entire frequency range [6]:

$$APR = \frac{Power\ in\ a\ specific\ frequency\ band}{Total\ power\ across\ all\ frequencies} \tag{17}$$

This measure provides insight into how well the network preserves physiologically relevant EEG frequency components while attenuating ECG artifacts.

III. Experiments and Results

This section presents the experimental validation of the proposed FD-DCNN framework. First, the data preparation process are discussed, followed by the details of the model training procedure. Finally, the performance is evaluated against baseline methods using multiple quantitative metrics.

III-A. Experimental Dataset

In this study, two publicly available datasets are employed to generate simulated data for model training and evaluation: the EEGdenoiseNet dataset [14], providing single channel clean EEG recordings, and the MIT-BIH Polysomnographic Database [30][31], containing single-lead ECG signals. As no publicly available dataset includes both naturally ECG-contaminated EEG and corresponding clean references, simulated datasets were generated to enable objective evaluation using the selected metrics. This approach aligns with standard practice in EEG denoising research [6][11][14][29] and ensures reproducibility under controlled SNR conditions. The EEG signals from EEGdenoiseNet were band-pass filtered between 1 Hz and 80 Hz to remove slow drifts and high-frequency noise, resampled to 256 Hz, and segmented into non-overlapping 4 second epochs ($N = 1024$). This segmentation length is selected through grid search optimization to balance denoising accuracy and computational efficiency. Similarly, the ECG recordings from the MIT-BIH Polysomnographic Database were filtered and resampled to 256 Hz to ensure temporal alignment with the EEG data, followed by segmentation into matching 4

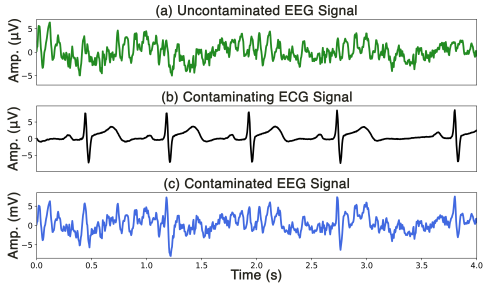

Figure 4. A segment of (a) Uncontaminated EEG, (b) Contaminating ECG, and (c) Contaminated EEG signal.

second epochs. This preprocessing ensured that both EEG and ECG datasets were time-synchronized and suitable for subsequent artifact mixing and model training. The ECG signals were then combined with clean EEG using the formula below [11]:

$$EEG_{noisy} = EEG_{clean} + \theta \cdot ECG \tag{18}$$

where θ is the mixing constant that regulates the signal-to-noise ratio (SNR) of the resulting noisy EEG signal, expressed as [14]:

$$SNR = 10 \log \frac{RMS(EEG_{clean})}{RMS(\theta \cdot ECG)} \tag{19}$$

where RMS is the root mean square of the signal. Previous studies on EEG artifact removal have reported that single channel EEG recordings contaminated by cardiac or physiological artifacts typically exhibit SNRs in the range of 5–15 dB [5][11][32][33]. This range is therefore adopted to generate realistic contamination levels for the simulated dataset. Figure 4 shows a segment of clean EEG, a contaminating ECG signal, and an EEG contaminated by an ECG signal. The dataset comprises 1,128 epochs across all three categories, which were randomly divided into training, validation, and test sets using an 80:10:10 split. All EEG inputs were standardized using z-score normalization for stable and consistent model training. Clean EEG epochs were used as ground-truth for evaluating the performance of the FD-DCNN.

III-B. Model Training

The FD-DCNN architecture was implemented using the Keras API with TensorFlow 2.0 framework and trained on a high-performance computing server equipped with an Intel Xeon Gold-6248 CPU (2.5 GHz), 192 GB DDR4-2933 MHz RAM, and an NVIDIA Tesla V100-PCIe GPU with 32 GB of VRAM. The training parameter and hyperparameter configurations are summarized in Table 1. The optimal hyperparameters were selected through a grid search based on validation performance. The network was trained using the proposed Morphology Preserving Loss (MPL), which simultaneously optimizes amplitude accuracy and preserves waveform morphology. Parameter updates during backpropagation were performed using the RMSprop optimizer with an adaptive learning rate schedule to ensure stable and efficient convergence. Figure 5 illustrates the training and validation loss curves for the proposed FD-DCNN model over 50 epochs, trained with a batch size of 32. Both curves exhibit a steep decline during the initial epochs, converging to around 0.0099 for the training loss and 0.0177 for the validation loss. The close alignment and smoothness of the training and validation loss curves arise from the synthetic, noise-controlled nature and statistically similar distribution of the simulated data, as well as the stable optimization behavior of the frequency domain architecture.

Table 1. The training parameters and hyperparameters for the proposed model.

Parameters/Hyperparameters	**Value**
Activation Function	PhaseReLU
Loss Function	MPL ($\lambda = 0.2$)
Optimizer	RMSprop
Learning Rate	0.0005
Batch Size	32
Epochs	50
Early Stopping	No
Weight Initializer	Glorot Uniform
Random Seed	42
Trainable Parameters	656, 010

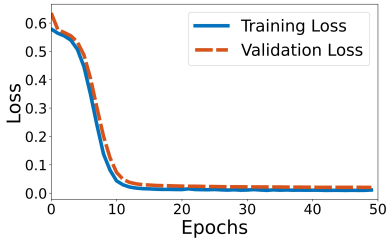

Figure 5. Training and validation loss curve comparison.

III-C. Performance Evaluation

The performance of the trained FD-DCNN model was quantitatively and qualitatively evaluated using the test dataset. Figure 6(a) and 6(b) show an example EEG segment in the temporal and spectral domains, respectively, illustrating the noisy, cleaned, and ground-truth signals. In the time domain plots, the reconstructed EEG waveform closely matches the ground-truth signal, effectively suppressing ECG-related distortions present in the contaminated input. In the frequency domain plots, the PSD of the cleaned EEG exhibits a substantial reduction in artifact-induced distortions while preserving the spectral characteristics of the ground-truth EEG. Time–frequency (TF) plots of EEG signals obtained using the Morlet wavelet transform are shown in Figure 7 to illustrate the distribution of signal power across time and frequency. The TF plots indicate that the noisy EEG is heavily contaminated by cardiac artifacts, particularly in the low-frequency band (1–20 Hz). The cleaned EEG generated by the FD-DCNN effectively suppresses these artifacts while preserving the essential

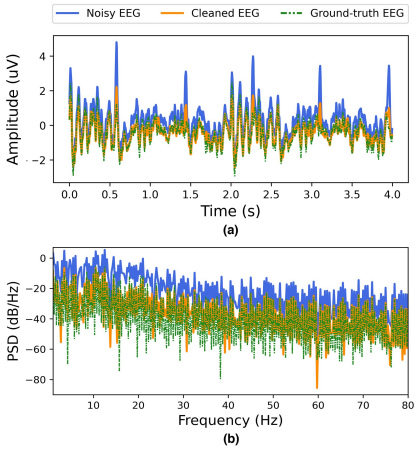

Figure 6. Reconstructed clean EEG by the FD-DCNN model in comparison with the noisy and ground-truth EEG, (a) Time domain, and (b) Frequency domain representation.

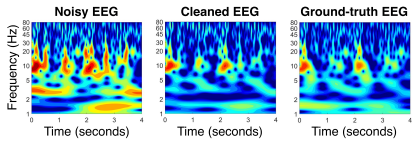

Figure 7. Time-frequency plots of noisy, cleaned, and ground-truth EEG, generated using Morlet wavelet transform.

temporal and spectral characteristics, closely matching the ground-truth signal.

For a consistent performance evaluation, a time domain CNN (TD-CNN) with an architecture identical in depth and filter configuration to FD-DCNN (32–64–128–64–32) was implemented as the baseline. Each layer employed 1-D convolutions with a kernel size of 9, ReLU activation, and residual skip connections at symmetric layers to mirror the structure of FD-DCNN. This design was selected to ensure that both models differ only in their convolutional domain (time vs frequency), thereby isolating the impact of Fourier domain processing on performance and computational efficiency. The baseline thus serves to validate the advantage of FD-DCNN in achieving comparable denoising accuracy with substantially reduced computational cost. Table 2 demonstrates significant advantages of FD-DCNN in both computational complexity and denoising efficacy. With only 0.67M parameters (vs. 33.67M), 2.5MB memory (vs. 128.42MB), and 2.31M FLOPs (vs. 290.39M), the FD-DCNN is much lighter, making it ideal for FPGA-based real-time EEG processing. Additionally, it achieves better cardiac artifact removal, with lower RRMSE in time (0.4301 vs. 0.5672) and frequency (0.3548 vs. 0.3748) domains, while maintaining higher signal correlation (0.8879 vs. 0.7674), confirming its effectiveness for portable EEG systems.

Table 2. Comparison of the proposed FD-DCNN with the baseline TD-CNN model.

Metrics	FD-DCNN	TD-CNN
Total parameters	0.67M	33.67M
Memory	2.50MB	128.42MB
FLOPs	2.31M	290.39M
Inference latency (GPU)	2.46 ms/seg	16.12 ms/seg
Throughput (GPU)	406.5 seg/s	62.03 seg/s
RRMSE_t	0.4301	0.5672
RRMSE_f	0.3548	0.3748
Correlation	0.8879	0.7674

Table 3. Average power ratios in different frequency bands for noisy EEG, cleaned EEG, and the ground-truth EEG signals.

Frequency Bands	Noisy EEG	Cleaned EEG	Ground-truth
Delta (1 – 4 Hz)	0.264	0.211	0.225
Theta (4 – 8 Hz)	0.168	0.151	0.163
Alpha (8 – 13 Hz)	0.314	0.440	0.426
Beta (13 – 30 Hz)	0.231	0.155	0.171
Gamma (30 – 80 Hz)	0.045	0.094	0.072

Table 4. Performance analysis of our proposed method.

Method	$\text{RRMSE}_t \downarrow$	$\text{RRMSE}_f \downarrow$	CC ↑
FCNN [14]	0.6832	0.6422	0.7266
Simple LSTM [14]	0.5668	0.5879	0.7951
Simple CNN [14]	0.5715	0.4826	0.8133
ResNet [26]	0.5497	0.4728	0.8379
1D-CDAE [29]	0.4622	0.4148	0.8442
FD-DCNN	**0.4301**	**0.3548**	**0.8879**

We further evaluated the proposed FD-DCNN against several baseline deep learning models, including Fully Connected Neural Network (FCNN) [14], simple CNN and Long Short-Term Memory (LSTM) [14], Residual Network (ResNet) [26], and Convolutional Denoising Autoencoder (1D-CDAE) [29], as summarized in Table 4. As no existing studies report comparable quantitative results for cardiac artifact removal in single channel EEG, we evaluated FD-DCNN against these models trained under identical conditions. Among these, CNN-based architectures consistently outperformed recurrent models such as LSTM, primarily due to their stronger capability to capture localized temporal structures of ECG artifacts and their more stable gradient propagation over long input sequences. FD-DCNN further advanced over conventional CNN performance by leveraging spectral-domain convolution, achieving the lowest RRMSE and highest correlation coefficient with substantially reduced computational complexity. These results confirm that performing convolution in the Fourier domain enables efficient, low-cost, and accurate EEG denoising suitable for real-time applications.

Table 3 reports the average power ratios across standard EEG frequency bands (Delta: 1–4 Hz, Theta: 4–8 Hz, Alpha: 8–13 Hz, Beta: 13–30 Hz, and Gamma: 30–80 Hz) for noisy, cleaned, and ground-truth signals. The cleaned EEG exhibits power ratios that closely align with the ground-truth across all bands. Alpha and Beta powers were most affected by cardiac artifacts; how-

Table 5. Ablation study showing the effect of PhaseReLU, MPL (λ variation), and skip connections on FD-DCNN performance.

Variant	RRMSE$_t$ ↓	RRMSE$_f$ ↓	Correlation ↑	Remarks
Baseline (PhaseReLU + MPL, $\lambda = 0.2$, with residuals)	0.4301	0.3548	0.8879	Full model
PhaseReLU only, without MPL ($\lambda = 0$, MSE only)	0.4653	0.3813	0.8671	Tests effect of correlation term in MPL
ReLU (real and imag), with MPL	0.5119	0.4155	0.8267	Tests effect of PhaseReLU by replacing with standard ReLU
λ variation ($0 - 1.0$)	0.4301	0.3548	0.8879	Sensitivity of MPL weight, best at $\lambda = 0.2$
No Residuals	0.4721	0.3853	0.8434	Tests skip-connection effect

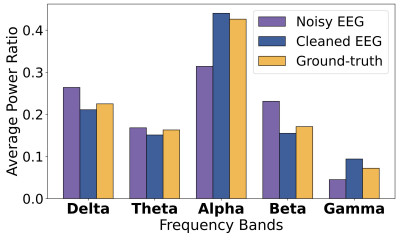

Figure 8. Bar plot for comparison of APR between noisy, cleaned, and ground-truth EEG in different frequency bands.

ever, the proposed method effectively restored them to near-ground-truth levels. Figure 8 shows a bar plot comparison of these ratios, demonstrating the method's ability to remove cardiac artifacts in single channel EEG while preserving essential spectral features.

To quantify the contribution of individual components, an ablation and sensitivity analysis is performed on PhaseReLU, the MPL, and the residual connections. As summarized in Table 5, removing the correlation term in MPL ($\lambda = 0$) or replacing PhaseReLU with a standard ReLU increased both temporal and spectral RRMSE while reducing correlation, confirming their importance in preserving EEG morphology and waveform fidelity. A sensitivity analysis through a grid search across $\lambda \in \{0, 0.05, 0.1, 0.2, 0.5, 1.0\}$ identified $\lambda = 0.2$ as the optimal trade-off between amplitude accuracy and morphological preservation. The exclusion of residual connections also degraded performance, emphasizing their role in stabilizing training and reconstruction.

IV. Conclusion

This paper introduced FD-DCNN, a Fourier domain convolutional neural network for efficient removal of cardiac artifacts in single channel EEG signals. By operating entirely in the spectral domain, the model replaces costly time domain convolutions with element-wise complex multiplications, significantly reducing computational complexity. Trained using the proposed Morphology Preserving Loss (MPL), FD-DCNN achieves superior denoising performance compared to a conventional time domain CNN, attaining lower RRMSE and higher correlation with fewer parameters, reduced memory requirement, and substantially lower FLOPs. With its lightweight architecture and superior performance over conventional CNN, FD-DCNN presents a promising solution for area and power efficient hardware implementation in real-time EEG processing. One limitation of this study is the use of synthetically generated EEG rather than naturally contaminated EEG recordings. Future work will focus on validating the proposed FD-DCNN on real EEG data and implementing it on FPGA and ASIC for real-time, low-power deployment in portable EEG systems.

Acknowledgements

We acknowledge the National Supercomputing Mission (NSM) for providing computing resources of 'Param-Kamrupa' at IIT Guwahati, which is implemented by C-DAC and supported by the Ministry of Electronics and Information Technology (MeitY) and Department of Science and Technology (DST), Government of India.

References

[1] M. X. Cohen, *Analyzing neural time series data: theory and practice*. MIT press, 2014.

[2] R. Acharjee and S. R. Ahamed, "EEG Data Augmentation Using Generative Adversarial Network for Improved Emotion Recognition," *International Conference on Pattern Recognition*. Springer, 2025, pp. 238–252.

[3] X. Jiang, G.-B. Bian, and Z. Tian, "Removal of artifacts from EEG signals: a review," *Sensors*, vol. 19, no. 5, p. 987, 2019.

[4] M. Nakamura and H. Shibasaki, "Elimination of EKG artifacts from EEG records: a new method of non-cephalic referential EEG recording," *Electroencephalography and clinical neurophysiology*, vol. 66, no. 1, pp. 89–92, 1987.

[5] C. Dora and P. K. Biswal, "Efficient detection and correction of variable strength ECG artifact from single channel EEG," *Biomedical Signal Processing and Control*, vol. 50, 2019.

[6] R. Acharjee and S. R. Ahamed, "Efficient muscle artifact removal from single channel eeg signals using deep long short-term memory network," *2024 IEEE 21st India Council International Conference (INDICON)*, 2024, pp. 1–6.

[7] M. M. N. Mannan *et al.*, "Identification and removal of physiological artifacts from electroencephalogram signals: A review," *Ieee Access*, vol. 6, pp. 30 630–30 652, 2018.

[8] S. F. Sheniha *et al.*, "Removal of artifact from EEG signal using differential evolution algorithm," *2013 International Conference on Communication and Signal Processing*. IEEE, 2013.

[9] J.-A. Jiang *et al.*, "An automatic analysis method for detecting and eliminating ECG artifacts in EEG," *Computers in biology and medicine*, vol. 37, no. 11, pp. 1660–1671, 2007.

[10] R. Patel *et al.*, "Common methodology for cardiac and ocular artifact suppression from EEG recordings by combining ensem-

ble empirical mode decomposition with regression approach," *Journal of Medical and Biological Engineering*, vol. 37, no. 2, pp. 201–208, 2017.

[11] C. Dora and P. K. Biswal, "Correlation-based ECG artifact correction from single channel EEG using modified variational mode decomposition," *Computer Methods and Programs in Biomedicine*, vol. 183, p. 105092, 2020.

[12] S. Behera *et al.*, "A Machine Learning Approach for Artifact Removal from Brain Signal." *Computer Systems Science & Engineering*, vol. 45, no. 2, 2023.

[13] B. Kalita *et al.*, "AnEEG: leveraging deep learning for effective artifact removal in EEG data," *Scientific Reports*, vol. 14, no. 1, p. 24234, 2024.

[14] H. Zhang, M. Zhao, C. Wei, D. Mantini, Z. Li, and Q. Liu, "EEGdenoiseNet: a benchmark dataset for deep learning solutions of EEG denoising," *Journal of Neural Engineering*, vol. 18, no. 5, p. 056057, 2021.

[15] Y. Han and B.-W. Hong, "Deep learning based on fourier convolutional neural network incorporating random kernels," *Electronics*, vol. 10, no. 16, p. 2004, 2021.

[16] H. Pratt *et al.*, "FCNN: Fourier Convolutional Neural Networks," *Joint European Conference on Machine Learning and Knowledge Discovery in Databases*. Springer, 2017, pp. 786–798.

[17] A. V. Oppenheim, *Discrete-time signal processing*. Pearson Education India, 1999.

[18] K. K. Parhi and M. Ayinala, "Low-Complexity Welch Power Spectral Density Computation," *IEEE Transactions on Circuits and Systems I: Regular Papers*, vol. 61, no. 1, 2014.

[19] R. Bracewell and P. B. Kahn, "The Fourier transform and its applications," *American Journal of Physics*, vol. 34, no. 8, pp. 712–712, 1966.

[20] J. W. Cooley and J. W. Tukey, "An algorithm for the machine calculation of complex Fourier series," *Mathematics of computation*, vol. 19, no. 90, pp. 297–301, 1965.

[21] A. Paul, S. Rafi Ahamed, and R. Paily Palathinkal, "Continuous Flow 4096-Point FFT/IFFT Hardware Architecture for 5G Applications," *IEEE Transactions on Circuits and Systems I: Regular Papers*, pp. 1–14, 2025.

[22] I. Sutskever, J. Martens, G. E. Dahl, and G. E. Hinton, "On the importance of initialization and momentum in deep learning," *International Conference on Machine Learning*, 2013.

[23] L. Chi, B. Jiang, and Y. Mu, "Fast fourier convolution," *Advances in Neural Information Processing Systems*, vol. 33, pp. 4479–4488, 2020.

[24] K. K. Parhi, "VLSI Digital Signal Processing Systems: Design and Implementation," *John Wiley & Sons*, 2007.

[25] A. Paul, S. R. Ahamed, and R. Paily Palathinkal, "Asic and fpga implementation of radix-22 32-point mdc-fft architecture," *2023 IEEE Silchar Subsection Conference (SILCON)*, 2023, pp. 1–6.

[26] K. He *et al.*, "Deep residual learning for image recognition," *2016 IEEE Conference on Computer Vision and Pattern Recognition (CVPR)*, pp. 770–778, 2015.

[27] S. Wang *et al.*, "Training deep neural networks on imbalanced data sets," *2016 International Joint Conference on Neural Networks (IJCNN)*, pp. 4368–4374, 2016.

[28] F. Kahraman *et al.*, "Correlation Loss: Enforcing Correlation between Classification and Localization," *AAAI Conference on Artificial Intelligence*, 2023.

[29] R. Acharjee and S. R. Ahamed, "Automatic Eyeblink Artifact Removal from Single Channel EEG Signals Using One-Dimensional Convolutional Denoising Autoencoder," *2024 International Conference on Computer, Electrical Communication Engineering (ICCECE)*, 2024, pp. 1–7.

[30] Y. Ichimaru and G. Moody, "Development of the polysomnographic database on CD-ROM," *Psychiatry and clinical neurosciences*, vol. 53, no. 2, pp. 175–177, 1999.

[31] A. L. Goldberger *et al.*, "PhysioBank, PhysioToolkit, and PhysioNet: components of a new research resource for complex physiologic signals," *circulation*, vol. 101, no. 23, 2000.

[32] D. B. Stone *et al.*, "Automatic removal of physiological artifacts in EEG: the optimized fingerprint method for sports science applications," *Frontiers in Human Neuroscience*, vol. 12, 2018.

[33] G. Tamburro *et al.*, "Automatic removal of cardiac interference (ARCI): A new approach for EEG data," *Frontiers in Neuroscience*, vol. 13, p. 441, 2019.